Supplementary Materials for Country distancing reveals the effectiveness of travel restrictions during COVID-19

Lu Zhong, Mamadou Diagne* Weiping Wang, Jianxi Gao*

Contents

1 Dataset

The global mobility network. The data for constructing the global mobility network (GMN) is provided by the Official Airline Guide (OAG). This dataset includes the airports and the seats of scheduled commercial flights between airports in 2013. We assumed that the daily scheduled commercial flights in 2020 are the same as in 2013. We also assume that the number of seats on the scheduled commercial flights is proportional to the number of passengers taking air travels. We construct the weighted and directed GMN by integrating the airports to corresponding geographic areas and integrating the passengers/seats between airports. We represent GMN as $G = (N, E, F)$, N is the set of $M = 228$ geographical areas, E is the set of $|E| = 5493$ airline links, and F is the passenger influx of airline links (see Table S1 and S2). F_{mn} is the number of passengers that travels from country n to country m, and $F_{mn} \neq F_{nm}$. The total amount of passenger influx is 7,259,935 passengers per day.

Geographic areas' infected cases and arrival times. According to the Johns Hopkins University (***?***), we obtain the reported infected cases, recovered cases, and death toll from Jan-22 to Apr-4 in 249 geographic areas. Combing the data set from Johns Hopkins University (*?*) and Ding Xiang Doctor Website (***?***), which published the daily fact-checking statements related to the outbreak, we obtain the arrival times of 199 areas as of Apr-4. Notably, we consider Dec-8 in 2019 as the arrival time of mainland China when the first case was reported.

Geographic areas' population. We collect the geographic areas‘ population in 2019 from the website World Population Review (***?***).

Travel Restrictions. Currently, 249 countries, territories, or areas of geographical interest that are assigned two-letter official codes in ISO 3166-1 are considered in the travel restrictions' dataset. The information about entry bans and global travel bans are collected from (***?***). The information about lockdowns is obtained from a summary of government measures regarding

COVID-19 from ACAPS in the Humanitarian Data Exchange website (***?***). Until Apr-4, 2020, 184 areas have imposed 476 entry bans, 87 areas imposed 87 global travel bans, and 70 countries imposed 100 lockdowns (see Table S3). Among the lockdowns, 12 geographic areas imposed 12 full lockdowns, and 65 geographic areas imposed 88 partial lockdowns.

2 SIR Meta-population Model

We adopt the SIR meta-population model to simulate the spread of COVID-19 in the global mobility network (GMN). For each geographic area n, it has a population size of Ω_n (from the 2019 world population statistics). The disease time course within the population is described by the three states (i.e., susceptible $s_n = S_n/\Omega_n$, infectious $i_n = I_n/\Omega_n$, recovered $r_n = R_n/\Omega_n$), and the disease time course between populations is described by their travels influx $p_{mn} = \frac{F_{mn}}{\sum_m F_{kn}}$:

$$\begin{cases} \dot{s}_n = -\alpha s_n i_n \sigma(i_n/\varepsilon) + \gamma \sum_{m \neq n} p_{mn}(s_m - s_n) \\ \dot{i}_n = \alpha s_n i_n \sigma(i_n/\varepsilon) - \beta i_n + \gamma \sum_{m \neq n} p_{mn}(i_m - i_n) \\ \dot{r}_n = \beta i_n + \gamma \sum_{m \neq n} p_{mn}(i_m - i_n) \end{cases} \tag{S1}$$

with the initial condition as

$$\dot{i}_k(t_0) = 1/\Omega_k, k \in N_I(t_0) \tag{S2}$$

where α is infectious rate, and $\alpha = R_0/D_I$. β is the recovery rate, and $\beta = 1/D_I$. D_I is the infectious period. R_0 is the basic reproductive number. $\gamma = \frac{\sum m,n F_{mn}}{\sum_n \Omega_n}$ ($\gamma = 0.010$) is the mobility rate. $\sigma(i_n/\varepsilon) = \frac{(i_n/\varepsilon)^\eta}{(i_n/\varepsilon)^\eta + 1}$ is a sigmoid Hill-type function. $\varepsilon \approx M/\sum_n \Omega_n = 3.242 * 0.1^7$. $N_I(t_0)$ is the set of outbreak locations (OL).

We simulate the global spread of COVID-19 by using the SIR meta-population model on GMN, with the basic reproductive number R_0 2.2 (95% CI, 1.4-3.9), the infectious period D_I 2.3 (95% CI, 1.2-12) provided by the literature (***?***), and $N_I(t_0) = \{\text{mainland China}\}$ where t_0 =Dec-8. Then, we get two fundamental properties – the arrival time (T_n) once the infected

cases $I_n(t) > 1$, and the infected cases ($I_n(t)$) in arbitrary geographic area n.

3 Country Distancing

Consider $\tau_{m|n} = \{n, c_1, ..., c_i, c_j, ..., c_k, m\}$ is the path of $L_{m|n}$ steps from (outbreak location) OL geographic area n to geographic area m in G, the probability of connects the two areas is

$$W(\tau_{m|n}) = P_{mc_k} \times, ..., P_{c_i c_j}, ..., \times P_{c_1 n}, \tag{S3}$$

where $P_{c_i c_j} = \frac{F_{c_i c_j}}{\sum_{c_i'} F_{c_i' c_j}}$ is the fraction of passenger influx from geographic area c_j to geographic area c_i over all out-flow influx from geographic area c_j. The effective distance of path $\tau_{m|n}$ from source area n to destination area m is

$$\begin{aligned} \lambda(\tau_{m|n}) &= L_{m|n} - logW(\tau_{m|n}) \\ &= \sum_{(i,j)\in\tau_{m|n}} (1 - logP_{ij}). \end{aligned} \tag{S4}$$

For arbitrary source area n and destination area m, the effective distance $d_{m|n}$ (***?***) is the minimal length of $\lambda(\tau_{m|n})$ for a path $\tau_{m|n}$, defined as

$$d_{m|n} = \min_{\tau_{m|n}} \lambda(\tau_{m|n}), \tag{S5}$$

which is the sum of effective distance of links in the path $\tau_{m|n}$, in par with the *effective effective resistance* in series circuits.

Assume we have multiple outbreak locations (OLs) $N_I = \{n_1, n_2, ..., n_i, ...\}$ and $|N_I| \geq 1$, so the probability of connecting from OLs N_I to destination m is:

$$\begin{aligned} W_m &= \frac{1}{M} \sum_{n_i \in N_I} W(\tau_{m|n_i}) \\ &= \frac{1}{M} \sum_{n_i \in N_I} \prod_{(i,j)\in\tau_{m|n_i}} P_{ij} \\ &= \frac{1}{M} \sum_{n_i \in N_I} e^{L_{m|n_i} - \lambda(\tau_{m|n_i})}, \end{aligned} \tag{S6}$$

where $M = |N|$ is the number of geographic areas in the GMN and is also the number of possible outbreak locations. $N_I \in N$, thus $W_m \leq 1$.

As each path $\tau_{m|n_i}$ is the path with minimal length from OL $n_i \in N_I$ to destination area m, then

$$W_m = \frac{1}{M} \sum_{n_i \in N_I} e^{L_{m|n_i} - d_{m|n_i}}. \tag{S7}$$

So the *country distancing* of area m, which quantifies how far country m is from multiple OLs $n_i \in N_I$, is:

$$D_{m|N_I} = L_{m|N_I} - log(\frac{1}{|M|} \sum_{n_i \in N_I} e^{L_{m|n_i} - d_{m|n_i}}) \tag{S8}$$

where

$$L_{m|N_I} = \min_{n_i \in N_I} L_{m|n_i}. \tag{S9}$$

Eq. S8 could also be represented as

$$\frac{e^{L_{m|N_I}}}{e^{D_{m|N_I}}} = \frac{1}{M} \sum_{n_i \in N_I} \frac{e^{L_{m|n_i}}}{e^{d_{m|n_i}}}. \tag{S10}$$

As $L_{m|N_I} \leq L_{m|n_i}$ for any $n_i \in N_I$, $L_{m|n_i} \leq d_{m|n_i}$ and $L_{m|n_i} \leq 3$, we have

$$e^{D_{m|N_I}} = \frac{M}{\sum_{n_i \in N_I} \frac{1}{e^{d_{m|n_i}}}} \tag{S11}$$

which similar to the *effective effective resistance* in parallel circuits. So the *country distancing* of area m could also be presented as

$$D_{m|N_I} = log(M) - log \sum_{n_i \in N_I} \frac{1}{e^{d_{m|n_i}}} \tag{S12}$$

For the explanations on notations and further calculations about *country distancing*, please check Table. S1.

4 Arrival Times and Infected Cases

4.1 Correlations with Country Distancing

According to existing literature, we know that the *effective distance* $d_{m|n}$ exhibits linear correlations with arrival times T_m (*?*) and the log-transformed mobility flow (the other form of *effective distance*, that is, $e^{L_{m|n}-d_{m|n}}$) exhibits linear correlation with log-transformed infected cases I_m (***?***) in the presence of one outbreak location (OL). *Country distancing*, a metric extended from *effective distance*, could also exhibit these two types of linear correlations in the presence of one/multiple outbreak locations. Specifically, as shown in Fig. S1A-C, the simulated arrival times $T_{m|N_I}$ could be well predicted by *country distancing* $D_{m|N_I}$ with $R^2 = 0.9$ for N_I=$\{$mainland China$\}$, $R^2 = 0.89$ for N_I=$\{$mainland China, Japan, South Korea, Italy$\}$, and $R^2 = 0.85$ for N_I having 119 geographic areas. As shown in Fig. S1. D-E, the log-transformed infected cases $log(I_{m|N_I})$ could be well predicted by *country distancing* $D_{m|N_I}$ (which is also log-transformed mobility flow $D_{m|N_I} \approx log(e^{-D_{m|N_I}}) \approx log(e^{L_{m|N_I}-D_{m|N_I}})$) with $R^2 = 0.91$ for N_I=$\{$mainland Chin$\}$, $R^2 = 0.90$ for N_I=$\{$mainland China, Japan, South Korea, Italy$\}$, and $R^2 = 0.77$ for N_I having 119 geographic areas.

But the *country distancing* fails to exhibit linear correlation with real-world infected cases and real-world infected cases, as shown in Fig. S2. Researchers point out that there are mass undetected, missing, undiagnosed, or unreported COVID-19 cases (***?, ?, ?, ?, ?***). For example, about 86% of infected cases were undocumented before travel restrictions in mainland China (*?*). The mass undetected cases result in biased arrival times and infected cases in the collected real-world dataset, and further make the real-world arrival times and infected cases unable to confirm the linear relationships with *country distancing*.

As the robustness check, we study the correlations between *country distancing* with simulated arrival times and simulated infected cases in the presence of different outbreak locations

$N_I(t)$, which is defined as the geographic areas whose infected case is more than 100, and $|1 \leq N_I(t) \leq 119|$ as of Apr-4. See Fig. S3, the linear correlations establish for different size of outbreak locations with $R^2 \in [0.83, 0.90]$ between *country distancing* and simulated arrival times and with $R^2 \in [0.77, 0.92]$ between *country distancing* and log-transformed infected cases. The slope v_{N_I} (measuring the change of arrival times relative to the change of *country distancing*) and the slope u_{N_I} (measuring the change of log-transformed infected cases relative to the change *country distancing*) are varied for different size of outbreak locations. To give the generic speeds of arrival times and infected cases from OLs, we estimate the average slope of v_{N_I} as $\bar{v}$ ($\bar{v} = 5.50$ [95% CI, 4.58 to 6.41)] and the average slope of v_{N_I} as $\bar{u}$ [$\bar{u} = -2.95$ (95% CI,-3.51 to -2.38)].

4.2 Arrival Time Delay and Infected Case Reduction

With $\bar{v} = 5.50$ (95% CI, 4.58 to 6.41) (slope for linear correlation between *country distancing* and arrival times) and $\bar{u} = -2.95$ (95% CI,-3.51 to -2.38) (slope for linear correlation between *country distancing* and log-transformed infected cases), we could calculate how the arrival times are delayed and the infected cases are reduced as the *country distancing* increases due to travel restrictions. Explicitly, the s^{th} travel restriction increases *country distancing* for area m by $D^{\star}_{m|F(t_s)}$, simultaneously, it would cause arrival time delay (ATD) $T^{\star}_{m|F(t_s)}$ and infected case reduction (ICR) $I^{\star}_{m|F(t_s)}$ for area m with following equations:

$$\begin{aligned} T^{\star}_{m|F(t_s)} &= \hat{v} D^{\star}_{m|F(t_s)}, \quad if \quad I_m(t_s) = 0 \\ I^{\star}_{m|F(t_s)} &= \sum\nolimits_{t \in \{t | t \in T, t \geq t_s \& N_I(t) = N_I(t_s)\}} \frac{D^{\star}_{m|F(t_s)} I^{\star}_m(t) (e^{-\hat{u} \times D^{\triangle}_m(t)} - 1)}{D^{\triangle}_m(t)} \end{aligned} \tag{S13}$$

We illustrate the procedures of calculating ATD and ICR (see algorithm 1 and algorithm 2) with the example $\{(1)^{th}$,$(2)^{th}$,$(3)^{th}\}$ travel restrictions in Fig. S4. The three example travel restrictions are imposed on {Jan-30, Jan-31, Jan-31} respectively, and cause {1,2,3} of $D^{\star}_{m|F(t_s)}$ respectively for area m when mainland China (CN) is the only outbreak location.

For the $(1)^{th}$ travel restriction, if the area m has not been infected on t_1 =Jan-30, then the ATD of area m is $T^{\star}_{m|F(t_1)} = 5.5 \times 1$ days; if the area m is infected on t_1=Jan-30, then $T^{\star}_{m|F(t_1)}$=0 days. Same procedure (algorithm 1) are applied to other travel restrictions.

Algorithm 1: Procedure of calculating arrival time delay (ATD).

input : G, $\bar{v} = 5.50$, $I_m(t)$, $D^{\star}_{m|F(t_s)}$
output: $T^{\star}_{m|F(t_s)}$, $T^{\star}_{G|F(t_s)}$

```
for s^th travel restriction do
    for m ∈ G do
        if I_m(t_s)=0 then
            T*_{m|F(t_s)} = v̂ D*_{m|F(t_s)}
        else
            T*_{m|F(t_s)} = 0
        end
    end
    T*_{G|F(t_s)} = Σ_{m∈G} T*_{m|F(t_s)} / M
end
```

As for ICR, we define the new infected case at area m as $I^{\star}_m(t) = I_m(t+1) - I_m(t)$. We firstly filter out the travel restrictions prior to time t and having the same OL set $N_I(t)$ and save them as S'. In our example travel restrictions, $S' = \{1^{th}\}$ on Jan-30, and $S' = \{1^{th}, 2^{th}, 3^{th}\}$ on Jan-31. Then, we calculate the accumulative increase of *country distancing* $D^{\triangle}_m(t)$ at area m brought by travel restriction in S'. $D^{\triangle}_m(t) = 1$ on Jan-30, and $D^{\triangle}_m(t) = 1 + 2 + 3 = 6$ on Jan-31 in our example. Next, we calculate area m's total reduced infected cases at time t caused by travel restriction in S'. $I^{temp}_m = I^{\star}_m(t)(e^{2.95 \times 1} - 1)$ on Jan-30, and $I^{temp}_m = I^{\star}_m(t)(e^{2.95 \times 6} - 1)$ on Jan-31 in our example. Next, we distribute the total reduced infected cases to travel restrictions according to their increase in *country distancing*. The ICR caused by $(1)^{th}$ travel restriction on Jan-30 is $\frac{1}{1} I^{\star}_m(t)(e^{2.95 \times 1} - 1)$, the ICR caused by $(1)^{th}$ travel restriction on Jan-31 is $\frac{1}{6} I^{\star}_m(t)(e^{2.95 \times 6} - 1)$. Applying the above four procedures to other travel restrictions, we could finally obtain area m's ICR caused by $(1)^{th}$ travel restriction by summing the daily produced

ICR for area m.

The reason of filtering out the travel restrictions having the same OL set is that the travel restrictions, which are imposed when fewer OLs appear, are not effective for the intertwined influence from new OLs. So, we ignore ICR caused by travel restrictions having the fewer OL set.

Algorithm 2: Procedure for calculating ICR.

input : G, T, $\bar{u} = -2.95$, $I_m(t)$, $D^{\star}_{m|F(t_s)}$
output: $I^{\star}_{m|F(t_s)}$, $I^{\star}_{G|F(t_s)}$

for $t \in T$ **do**
  list $S' = [\,]$;
  for s^{th} *travel restriction* **do**
    if $t_s \leq t$ *and* $N_I(t) = N_I(t_s)$ **then**
      list $S' = S' + [s]$;
    end
  end
  for $m \in G$ **do**
    $D^{\triangle}_m(t) = 0$;
    for $s'^{th} \in S'$ *travel restriction* **do**
      $D^{\triangle}_m(t) += D^{\star}_{m|F(t_{s'})}$;
    end
    $I^{\star}_m(t) = I_m(t+1) - I_m(t)$;
    $I^{temp}_m = I^{\star}_m(t)(e^{-\hat{u} \times D^{\triangle}_m(t)} - 1)$;
    for $s'^{th} \in S'$ *travel restriction* **do**
      $I^{\star}_{m|F(t_{s'})} += \frac{D^{\star}_{m|F(t_{s'})}}{D_m(t)^{\triangle}}$
    end
  end
end
for s^{th} *travel restriction* **do**
  $I^{\star}_{G|F(t_s)} = \sum_{m \in G} I^{\star}_{m|F(t_s)}/M$
end

5 Existing Travel Restrictions

5.1 Effectiveness of Travel Restrictions

By assuming the strengths of passenger influx reduction (α, β, and γ) for the three types of travel restrictions, i.e., $\alpha = 50\%$ for entry bans, $\beta = 90\%$ for global travel bans, $\gamma = 10\%$ for partial lockdowns and $\gamma = 90\%$ for full/national lockdowns, we obtain the increase in *country distancing* for each travel restriction. See Tab. S3, 337 (50.8%) travel restrictions make zero contribution in average *country distancing* $D^{\star}_{G|F(t_s)}$ for the world. Among the 337 entry bans, which induce zero $D^{\star}_{G|F(t_s)}$, 315 of them are entry bans to areas which are not OLs. Though the rest 22 of them are imposed on OLs, no actual links exit in GMN and thus lead to no increase in average *country distancing*. 304 travel restrictions induce $(0, 0.01]$ increase in average *country distancing*. Among the all 663 travel restrictions, only 22 (3.3%) of them make > 0.01 increase in $D^{\star}_{G|F(t_s)}$, and only 3 of them make > 0.1 increase in $D^{\star}_{G|F(t_s)}$. The three are Hubei's (a province in mainland China) lockdown with $D^{\star}_{G|F(t_s)} = 0.09$, mainland China's national lockdown with $D^{\star}_{G|F(t_s)} = 2.09$, and Italy's lockdwon with $D^{\star}_{G|F(t_s)} = 0.69$. Through the 663 travel restrictions, the final increase of $D^{\star}_{G|F(t_s)}$ is 3.869.

Tab. S5 summarized the total reduced influx, the average increase in *country distancing*, the average ATD, and the average ICR for the world bought by entry bans, global travel bans, and lockdowns. Overall speaking, lockdowns are most effective in increasing *country distancing*, ATD, and ICR. Entry bans are most effective and economical, produces more increase in *country distancing* than global travel ban with much less passenger influx. Excluding the travel restrictions whose $D^{\star}_{G|F(t_s)} = 0$, Fig. S5 shows the increase in *country distancing* caused by travel restrictions for two groups. One is the increase in *country distancing* ($D^{\star}_{n_s|F(t_s)}$) for area n_s, which imposed the travel restriction s, the other is the average increase in *country distancing* ($D^{\star}_{G|F(t_s)}$) for the world. Entry bans to mainland China have a higher increase in *country dis-*

tancing than entry bans to other areas. Fig S6 shows the arrival time delay (ATD) and infected case reduction (ICR) caused by travel restrictions, and their distributions. Observing Tab. S5, Fig. S5, and Fig. S6, we find that entry bans perform well in ATD and ICR with a small portion of reduced influx. It suggests that wisely deploy the entry bans could achieve the goal of effectively lowering the importation risk of COVID-19 and preserving the maximal passenger influx in GMN.

5.2 Areas' Gain and Contribution

Fig. S7, supplementary figure to Fig. 3B in the main text, shows areas' the arrival times delay (ATD) and infected case reduction (ICR) with travel restrictions till Feb-4, Mar-4, and Apr-4. Tab. S7 also lists the top ten geographic areas with the highest ATD and top ten geographic areas with the highest ICR.

Fig. S8 and Fig. S9, supplementary figure to Fig. 4 in main text, present each area's contribution of ATD and ICR to other continents, and continents' contribution of ATD and ICR to other continents.

6 Recommendations for Travel Restrictions

6.1 Optimization Travel Restrictions

As a supplementary to the optimized travel restrictions in the main text, we introduce the case when the optimized solutions would influence fewer airline links than existing travel restrictions, and simultaneously, keeping high effectiveness and minimizing the loss of passenger influx. Different from the bi-objective optimisation formulation in the main text, the size of

selected airline links for optimized travel restriction is $|\theta^{s'}| = K$,

$$\begin{aligned} \max_{\theta^{s'} \in \Theta^{s'}} \quad & \frac{\sum_{m,n} F_{mn}(t_{s'})}{\sum_{m,n} F_{mn}(t_0)} \\ \max_{\theta^{s'} \in \Theta^{s'}} \quad & D^{\star}_{G|F(t_{s'})} \\ \text{s.t.} \quad & F_{ij}(t_{s'}) = F_{i,j}(t_{s'-1})(1-\alpha), (i,j) \in \theta^{s'} \\ & F_{ij}(t_{s'}) = F_{i,j}(t_{s'-1}), (i,j) \notin \theta^{s'} \\ & \theta^{s'} \in E \& |\theta^{s'}| = K \end{aligned} \tag{S14}$$

We use the Non-dominated Sorting Genetic Algorithm (NSGA-II) to obtain non-dominated solutions when one OL (mainland China) and four OLs (mainland China, South Korea, Japan, and Italy) are presented with $\alpha = 0.5$ and $\alpha = 0.9$, respectively. When the OL is mainland China and $\alpha = 0.5$ (see Fig. S10A), we could easily get an optimal solution, which only reduces the passenger influx by 0.32% and enables 0.661 in increasing *country distancing* by involving 100 edges. In comparison with the existing travel restrictions imposed by Feb-6 (0.9% of reduced passenger influx, 0.39 increase in *country distancing*, and involving 268 edges), the optimal solution rises passenger influx by more than 0.58%, increases 69.48% in *country distancing*, and inflicts 168 less edges. For all optimal solutions, we notice that larger K induces a growth of the percentage of reduced passenger influx and enlarges *country distancing*.

From our analysis, when $\alpha = 50\%$, there exist no solutions that outperform the existing travel restrictions imposed by Feb-17, date after which mainland China imposed national lockdown (5.1% of passenger influx reduction, 2.687 increase of *country distancing*, and involving 443 edges). This observation is related to our assumption that national lockdowns reduce 90% of passenger influx for each edge, but optimal solution based on entry bans reduces only $\alpha = 50\%$ of passenger influx for each edge. Even if the optimal solutions based on entry bans have inflicted the same set of edges with the national lockdowns, the optimal solutions are worse in increase of *country distancing*.

From Fig S10.B, it can be seen that increasing α from 50% to 90%, the optimal solution (0.6% of decreased passenger influx, 2.264 increase of *country distancing* by involving only 100 edges) outperforms existing travel restrictions imposed by Feb-17 in decreased passenger influx and involved edges. More precisely, the passenger influx rises by 4.5%, and 343 less edges are inflicted. However, an increase of 2.27 in *country distancing*, 15.7% less than the existing travel restrictions imposed by Feb-17. To conclude, the NSGA-II enables us to find the optimal solutions that outperform the existing travel restrictions with a maximal increase of *country distancing*, a minimal decrease passenger influx, and a minimal inflicted edges by adjusting the strengths, α.

When four OLs $\{$mainland China, South Korea, Japan, and Italy$\}$ are presented on Feb-23 in S10.C-D, Italy imposed lockdowns with 2.8% of decrease in passenger influx, 0.165 increase in *country distancing*, and involving 191 edges. The optimal solutions obtained by NSGA-II are more effective than Italy's lockdown for $\alpha = 0.5$ and $\alpha = 0.9$. The optimal solution achieves almost the same with *country distancing*, 0.161, with a decrease of 1.1% in passenger influx, but inflicts 300 edges, when $\alpha = 0.5$. For $\alpha = 0.9$, the optimal solution outperforms Italy's lockdown with 0.23 increase of *country distancing*, augmenting the passenger influx by 1.8% with only 100 edges.

The obtained optimal solutions consist of a set of entry bans. To explore whether the set of entry bans in different optimal solutions share same features, we test the correlations between the number of entry bans targeting OLs (restricting the passenger influx has OLs) and the increase of *country distancing* in Fig. S11. Results prove that the number of entry bans targeting OLs have linear relationship with the increase*country distancing*. For instance, with $\alpha = 0.5$, when the OL is mainland China, a statistical coefficient $R^2 = 0.86$ is deduced while for the case of multiple OLs, namely, mainland China, Japan, South Korea, and Italy, the statistical coefficient is $R^2 = 0.96$ for the same value of α. With $\alpha = 0.9$, when the OL is mainland

China, a statistical coefficient $R^2 = 0.82$ is deduced while for the case of multiple OLs, namely, mainland China, Japan, South Korea, and Italy, the statistical coefficient is $R^2 = 0.94$.

In a nutshell, all the optimized solutions reveal that a small set of entry bans could achieve substantial increase of *country distancing* regardless of the number of outbreak locations. Moreover, based on the linear relationship between the number of entry bans targeting OLs and the increase of *country distancing*, our findings suggest that the most effective and direct way of distancing areas is to implement entry bans to OLs, without considering the intertwined spreading routes in the complex network.

Table S1: Table of Notation.

Notation	Description	
G	Global mobility network	$G = (N, E, F)$
N	Set of geographic areas	$\|N\| = M = 228$
E	Set of airline links between geographic areas	$\|E\| = 5493$
F	Set of passenger influx between geographic areas	$F(t_0) = F$, $F(t_s)$ for s^{th} travel restriction
$I_m(t)$	Infected cases in area m at time t	$t \leq$ Apr-4
$T_m(t)$	Arrival time in area m at time t	$t \leq$ Apr-4
$N_I(t)$	Set of outbreak locations	$N_I(t) = \{n \| \forall n \in N \& I_n(t) > 100\}$, $N_I \in N$, and $N_I(t_s)$ for s^{th} travel restriction
N_I'	Set of different outbreak locations	$N_I' = \{N_I(t) \| \forall t, N_I(t) \neq N_I(t+1)\}$
T	Set of dates for collected travel restrictions	$T =$ {Jan-21, Jan-22,....,Apr-4 }
$\mathbb{S}$	Set of occurrence orders of travel restrictions	$\mathbb{S} = \{1, 2, ..., s, ..., S\}$ and $\|S\| = 663$
$\mathbb{T}$	Set of the occurrence dates of travel restrictions	$\mathbb{T} = \{t_1, t_2, ..., t_s, ..., t_S\}$ and $t_s \in T$
$\mathbb{N}$	Set of countries which imposed s^{th} travel restriction	$\mathbb{N} = \{n_1, n_2, ..., n_s, ..., n_S\}$ and $n_s \in N$
$\mathbb{E}$	Set of airline links whose passenger influx are reduced by s^{th} travel restrictions	$\mathbb{E} = \{E_1, E_2, ..., E_s, ..., E_S\}$ and $E_s \in E$
α	Strength of entry ban	$\alpha = 50\%$
β	Strength of global travel ban	$\beta = 90\%$
γ	Strength of lockdown	$\gamma = 10\%$ for partial lockdown and $\gamma = 90\%$ for full lockdown
$d_{m\|n}$	Effective distance from n to m	$m, n \in N$
$D_{m\|N_I}$	*Country distancing* from N_I to m	
v_{N_I}	Speed of arrival time when N_I presents	$T_m = v_{N_I} \times D_{m\|N_I} + v_{0N_I}$, $\bar{v} = \frac{\sum_{N_I(t) \in N_I'} v_{N_I(t)}}{\|T\|}$
u_{N_I}	Speed of infected cases when N_I presents	$log(I_m) = u_{N_I} \times D_{m\|N_I} + u_{0N_I}$, $\bar{u} = \frac{\sum_{N_I(t) \in N_I'} u_{N_I(t)}}{\|T\|}$
$D_{m\|(N_I(t_s),F(t_s))}$	*Country distancing* in geographic area m when s^{th} travel restriction is implemented and set of outbreak locations $N_I(t_s)$ presents	$D_{m\|(N_I(t_s),F(t_s))} = D_{m\|N_I(t_s)} + D_{m\|F(t_s)}$
$D_{m\|F(t_s)}$	Area m's *country distancing* exclusively resulting by s^{th} travel restriction	
$D_{m\|N_I(t_s)}$	Area m's the *country distancing* resulting from outbreak locations	
$D_{G\|F(t_s)}$	Average *country distancing* resulting from by s^{th} travel restriction in G	$D_{G\|F(t_s)} = \frac{1}{M} \sum_{m \in N} D_{m\|F(t_s)}$
$D^{\star}_{m\|F(t_s)}$	Area m's increase in *country distancing* resulting from s^{th} travel restriction	$D^{\star}_{m\|F(t_s)} = D_{m\|F(t_s)} - D_{m\|F(t_{s-1})}$
$D^{\star}_{G\|F(t_s)}$	Average increase in *country distancing* resulting from s^{th} travel restriction	$D^{\star}_{G\|F(t_s)} = \frac{1}{M} \sum_{m \in N} D^{\star}_{m\|F(t_s)}$
$D^{\triangle}_m(t)$	Area m's accumulative increase in *country distancing* resulting from travel restrictions by time t	$D^{\triangle}_m(t) = \sum_{t_s \leq t} D^{\star}_{m\|F(t_s)}$
$D^{\triangle}_G(t)$	Worldwide average accumulative increase of *country distancing* resulting from travel restrictions by time t	$D^{\triangle}_G(t) = \frac{1}{M} \sum_{m \in N} D^{\triangle}_m(t)$
$D^{\triangledown}_n(t)$	Area n's accumulative contribution in increasing *country distancing* by imposing travel restrictions by time t	$D^{\triangledown}_n(t) = \sum_{n_s = n, t_s \leq t} D^{\star}_{G\|F(t_s)}$
$(T^{\star}_{m\|F(t_s)}, I^{\star}_{m\|F(t_s)})$	Area m's arrival time delay (ATD) and infected case reduction (ICR) caused by s^{th} travel restriction	see main text
$(T^{\star}_{G\|F(t_s)}, I^{\star}_{G\|F(t_s)})$	Worldwide average (ATD,ICR) resulting from s^{th} travel restriction	$T^{\star}_{G\|F(t_s)} = \frac{\sum_{m \in N} T^{\star}_{m\|F(t_s)}}{M}$, $I^{\star}_{G\|F(t_s)} = \frac{\sum_{m \in N} I^{\star}_{m\|Ft_s)}}{M}$
$(T^{\triangle}_m(t), I^{\triangle}_m(t))$	Area m's accumulative (ATD,ICR) resulting from travel restrictions by time t	$T^{\triangle}_m(t) = \sum_{t_s \leq t} T^{\star}_{m\|F(t_s)}$, $I^{\triangle}_m(t) = \sum_{t_s \leq s} I^{\star}_{m\|F(t_s)}$
$(T^{\triangle}_G(t), I^{\triangle}_G(t))$	Worldwide average accumulative (ATD,ICR)) resulting from travel restrictions by time t	$T^{\triangle}_G(t) = \frac{\sum_{m \in N} T^{\triangle}_m(t)}{M}$, $I^{\triangle}_G(t) = \frac{\sum_{m \in N} I^{\triangle}_m(t)}{M}$
$(T^{\triangledown}_n(t), I^{\triangledown}_n(t))$	Area n's accumulative contribution of (ATD,ICR) by imposing travel restrictions by time t	$T^{\triangledown}_n(t) = \sum_{n_s = n, t_s < t} T^{\star}_{G\|F(t_s)}$,$I^{\triangledown}_n(t) = \sum_{n_s = n, t_s < t} I^{\star}_{G\|F(t_s)}$

Table S2: Statistics of the global airline network. The columns from left to right are, the number of geographic areas, links, total passenger flux in the network, mean flux per link, mean in-degree of geographic areas, mean out-degree of geographic areas.

Airline	M	$\|E\|$	$\Phi[d^{-1}]$	$< F > [d^{-1}]$	$< K_{in} > [d^{-1}]$	$< K_{out} > [d^{-1}]$
G	228	5493	7259934	1321	48.3	45.8

Table S3: Travel restrictions implemented by Apr-4.

Travel restrictions	Entry ban	Global travel ban	full Lockdown	partial Lockdown
# of travel restrictions (663)	476 (71.7%)	87 (13.1%)	12 (18.1%)	88 (13.2%)
# of geographic areas imposing travel restrictions (249)	184 (73.8%)	87 (34.9%)	12 (4.8%)	65 (26.1%)

Table S4: Travel restrictions' average increase in *country distancing* worldwide $D^{\star}_{G|F(t_s)}$. $^{\diamond_1}$ represents the ten entry bans, namely, {HK-CN,US-CN,AT-CN,BE-CN,DE-CN,NL-CN,NZ-CN,TR-CN,AU-CN,RU-CN,US-JP}. $^{\diamond_2}$ represents {*CL,*KE,*AE,*NZ,*AU,*FJ,*NC}.

$D^{\star}_{G|F(t_s)}$	0	(0,0.01]	(0.01,0.1]	≥ 0.1
# of entry bans	333	133	$10^{\diamond_1}$	0
# of global travel bans	1	79	$7^{\diamond_2}$	0
# of lockdowns	3	92	2 (@ES,@ZA)	3(@Hubei,CN; @IT;@CN)
Total	337	304	19	3
Reduced influx	32,663 (1.3%)	1,331,292 (55.8%)	609,611 (25.58%)	409,482 (17.18%)

Table S5: The average increase in average *country distancing* $D^{\star}_{G|F(t_s)}$, average ATD $T^{\star}_{G|F(t_s)}$, and average ICR worldwide $I^{\star}_{G|F(t_s)}$ generated by three types of travel restrictions.

Travel restrictions	Reduced influx	$D^{\star}_{G|F(t_s)}$	$\frac{\sum_s D^{\star}_{G|F(t_s)}}{\sum_s 1}$	$T^{\star}_{G|F(t_s)}$	$\frac{\sum_s T^{\star}_{G|F(t_s)}}{\sum_s 1}$	$\sum_s I^{\star}_{G|F(t_s)}$	$\frac{\sum_s I^{\star}_{G|F(t_s)}}{\sum_s 1}$
entry bans	107,139	0.329	0.00069	1.53	0.0032	668.49	1.404
global travel bans	1,237,033	0.425	0.004	0.608	0.006	171.84	1.975
lockdowns	1,038,864	3.11	0.031	14.55	0.145	4188.69	41.88
Total	2,383,049	3.869	-	16.69	-	5029.03	-

Table S6: The top ten areas with the highest ATD, and the top ten areas with the highest ICR.

code	Geographic Area Name	ATD	code	Geographic Area Name	ICR
TV	Tuvalu	36.65	HK	Hong Kong	394,976
KP	North Korea	35.39	KR	South Korea	218,800
TM	Turkmenistan	31.62	IT	Italy	160,766
SL	Sierra Leone	29.62	JP	Japan	97,292
AL	Albania	29.58	TW	Taiwan	85,606
SV	El Salvador	29.35	SG	Singapore	63,278
MT	Malta	29.33	US	United States	42,984
LU	Luxembourg	29.23	DE	Germany	32,551
RO	Romania	28.91	IR	Iran	30,806
MD	Moldova	28.87	VN	Vietnam	28,304

Table S7: The top ten areas contribute the highest ATD to the world, and the top ten areas contribute the highest ICR to the world.

code	Geographic Area Name	ATD	code	Geographic Area Name	ICR
CN	mainland China	2,659	CN	mainland China	1,012,233
IT	Italy	868	HK	Hong Kong	88,526
US	United States	103	IT	Italy	47,004
AU	Australia	51	TW	Taiwan	18,931
NZ	New Zealand	46	TR	Turkey	14,548
NL	Netherlands	428	ES	Span	8,700
RU	Russia	36	US	United States	8,449
ZA	South Africa	32	DE	Germany	7,812
DE	Germany	28	VN	Vietnam	6,400
BE	Belgium	22	BR	Brazil	2,918

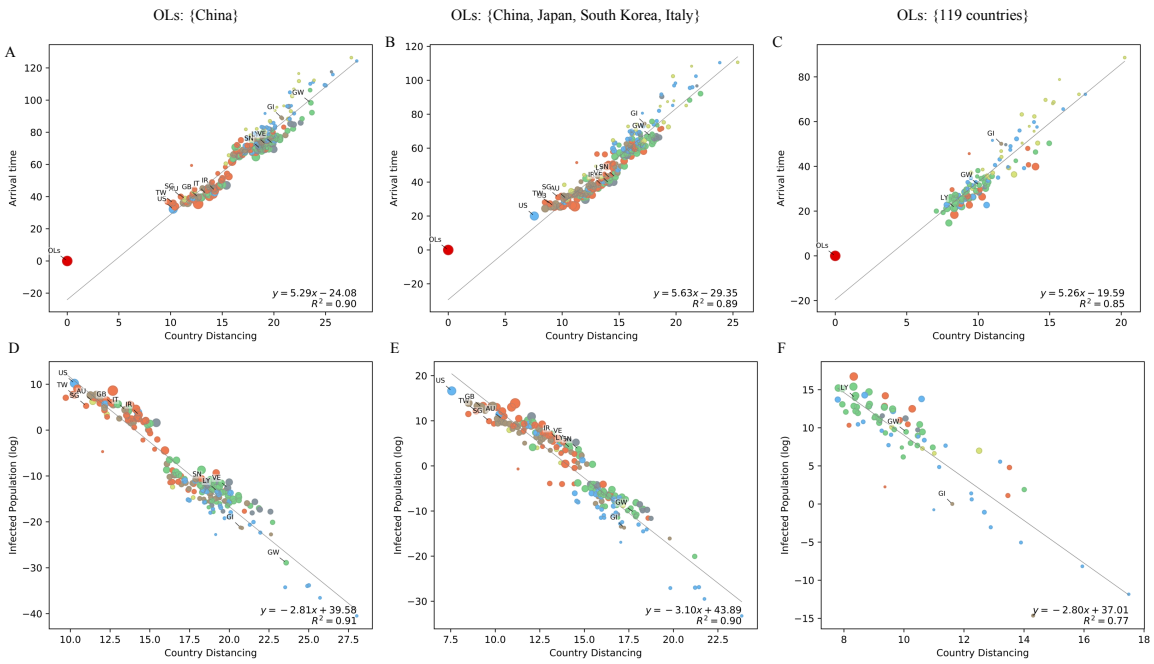

Figure S1: Correlation between *country distancing* $D_{m|N_I}$ and simulated arrival time T_m, and correlation between *country distancing* $D_{m|N_I}$ and simulated infected cases I_m for the pandemic COVID-19. The three columns are for when only {mainland China} is the OL, {mainland China, Japan, South Korea, Italy} are the OLs, and 119 areas are OLs as of Apr-4.

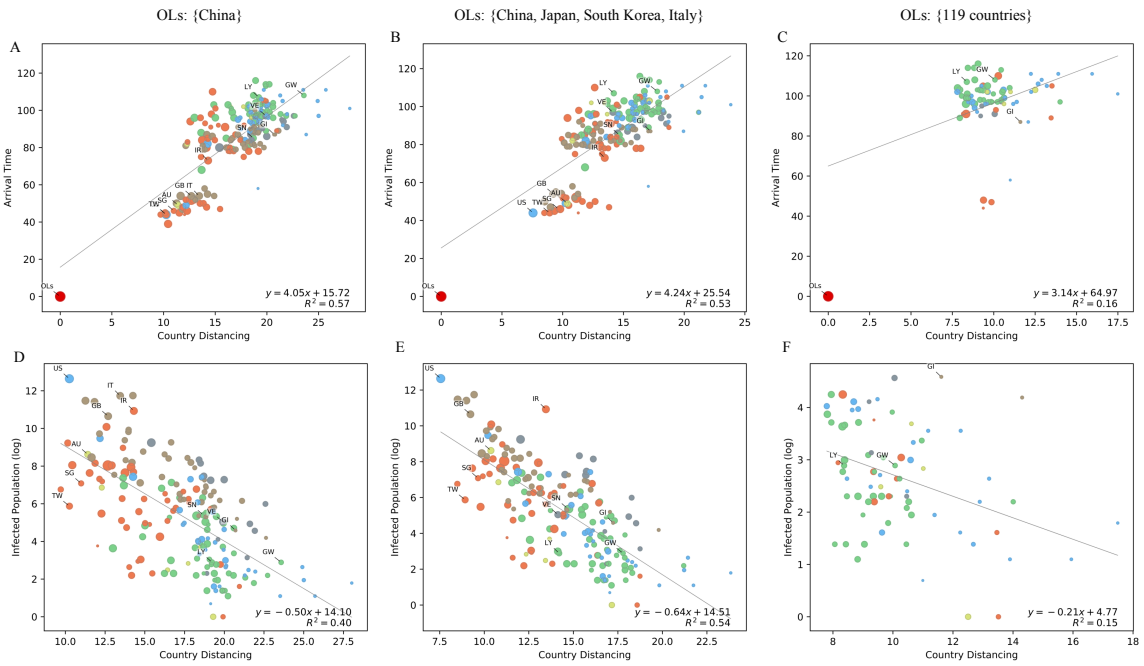

Figure S2: Correlation between *country distancing* $D_{m|N_I}$ and real-world arrival time T_m, and correlation between *country distancing* $D_{m|N_I}$ and real-world infected cases I_m for the pandemic COVID-19. The three columns are for when only {mainland China} is the OL, {mainland China, Japan, South Korea, Italy} are the OLs, and 119 areas are OLs as of Apr-4.

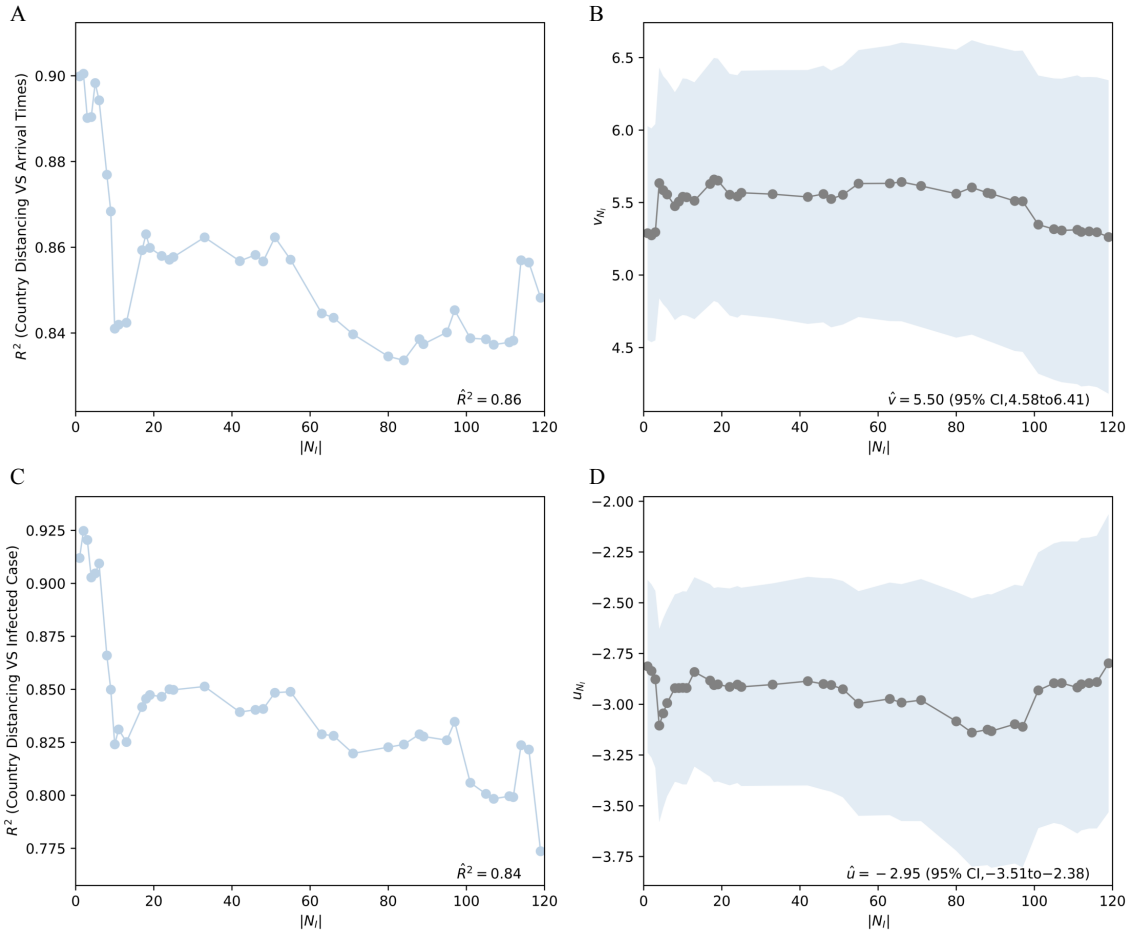

Figure S3: R-squared values for measuring the linear correlations between *country distancing* and arrival time / infected cases for the growing outbreak location set, and the corresponding slopes of formulation describing the linear correlations. (A) R-squared values and (B) slopes for linear correlation between *country distancing* and arrival time. (C) R-squared values and (D) slopes for linear correlation between *country distancing* and arrival time.

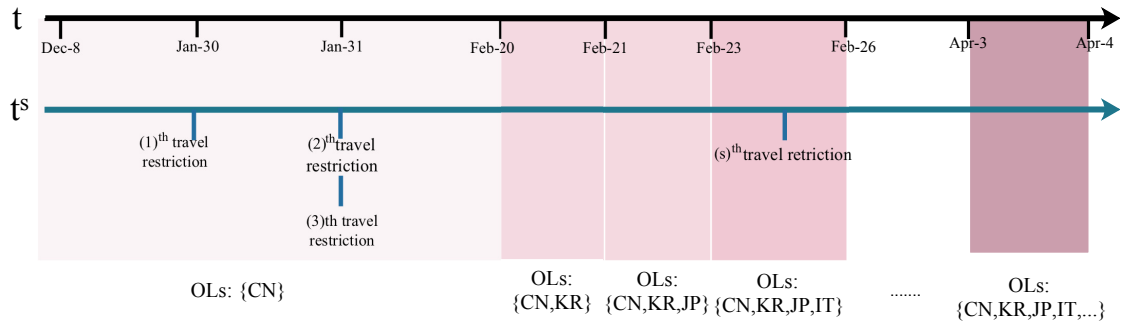

Figure S4: Timeline of example travel restrictions.

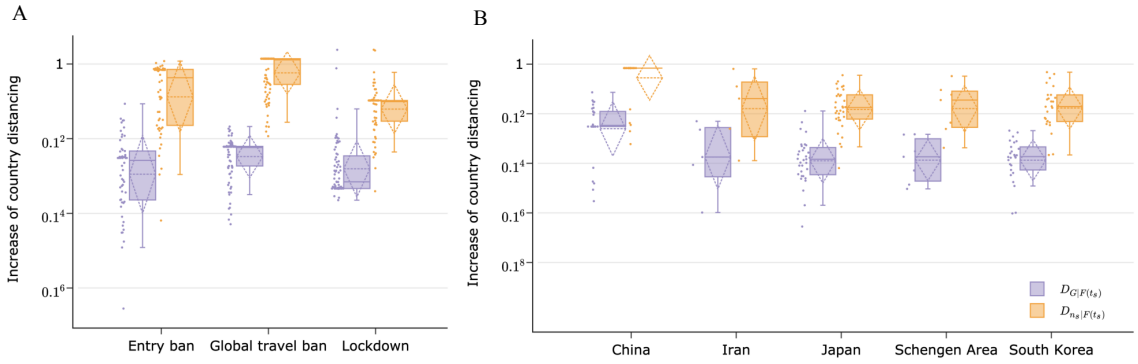

Figure S5: Increase in *country distancing* caused by travel restrictions. (A) Three main types of travel restrictions (i.e., entry ban, global travel ban, and lockdown). (B) Entry bans mainly to five areas, i.e., mainland China, Iran, Japan, Schengen Area, South Korea. $D^{\star}_{n_s|F(t_s)}$ represents the increase in *country distancing* in area n_s, which impose s^{th} travel restriction. $D^{\star}_{G|F(t_s)}$ represents the average increase in *country distancing* for the world. The travel restrictions whose $D^{\star}_{n_s|F(t_s)} = 0$ are not displayed here.

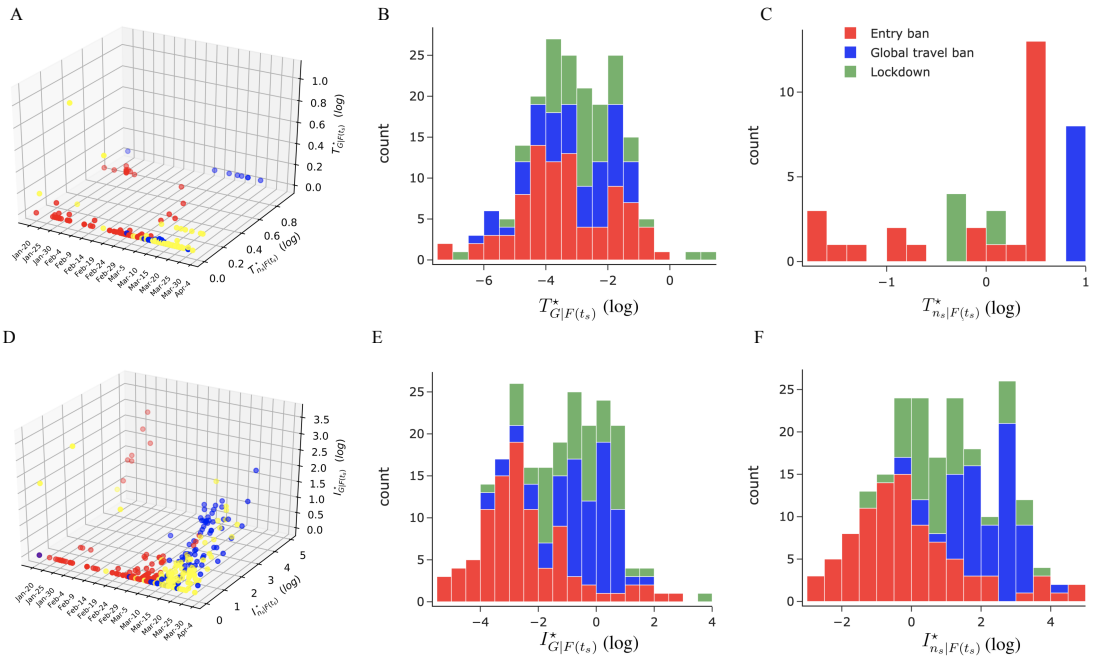

Figure S6: The arrival time delay (ATD) and infected case reduction (ICR) caused by travel restrictions. (A)(B)(C) The three-dimensional plots visualized the imposed time, average ATD ($T^{\star}_{G|F(t_s)}$) for the world [distribution in (B)] and the ATD ($T^{\star}_{n_s|F(t_s)}$) for area n_s [distribution in (C)], who imposed s^{th} travel restriction. (D)(E)(F) The three-dimensional plots visualized the imposed time, average ICR ($T^{\star}_{G|F(t_s)}$) for the world [distribution in (E)] and the ICR ($T^{\star}_{n_s|F(t_s)}$) for area n_s [distribution in (F)].

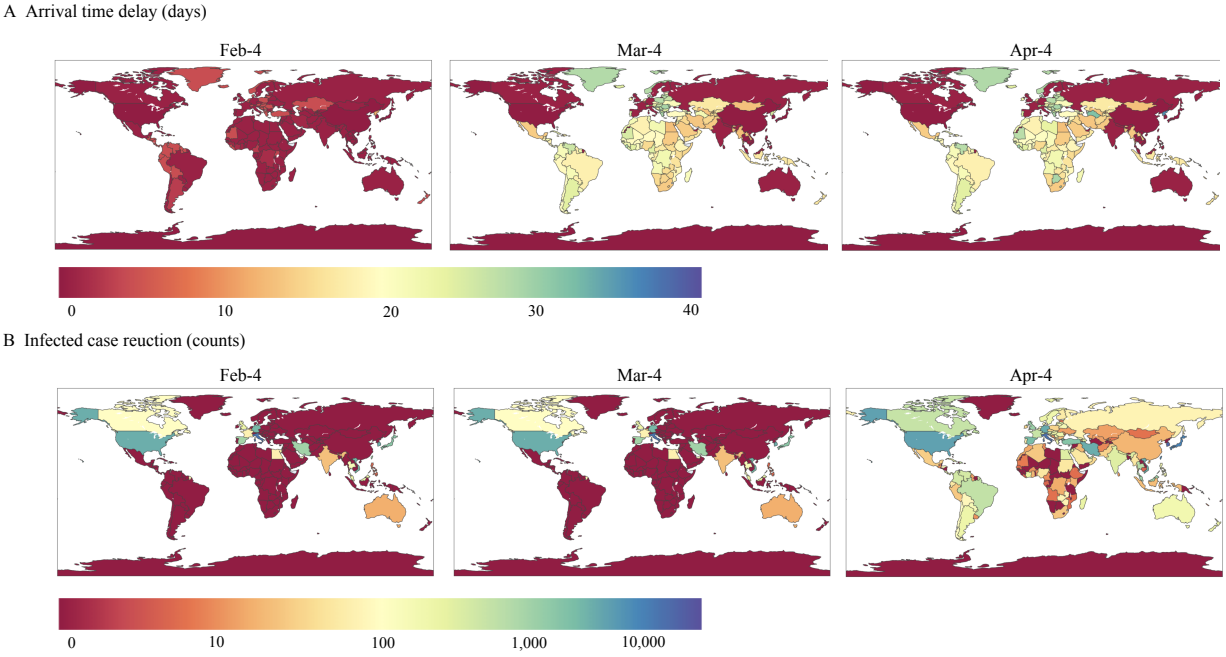

Figure S7: Areas' gain of arrival time delay (A) and infected case reduction (B).

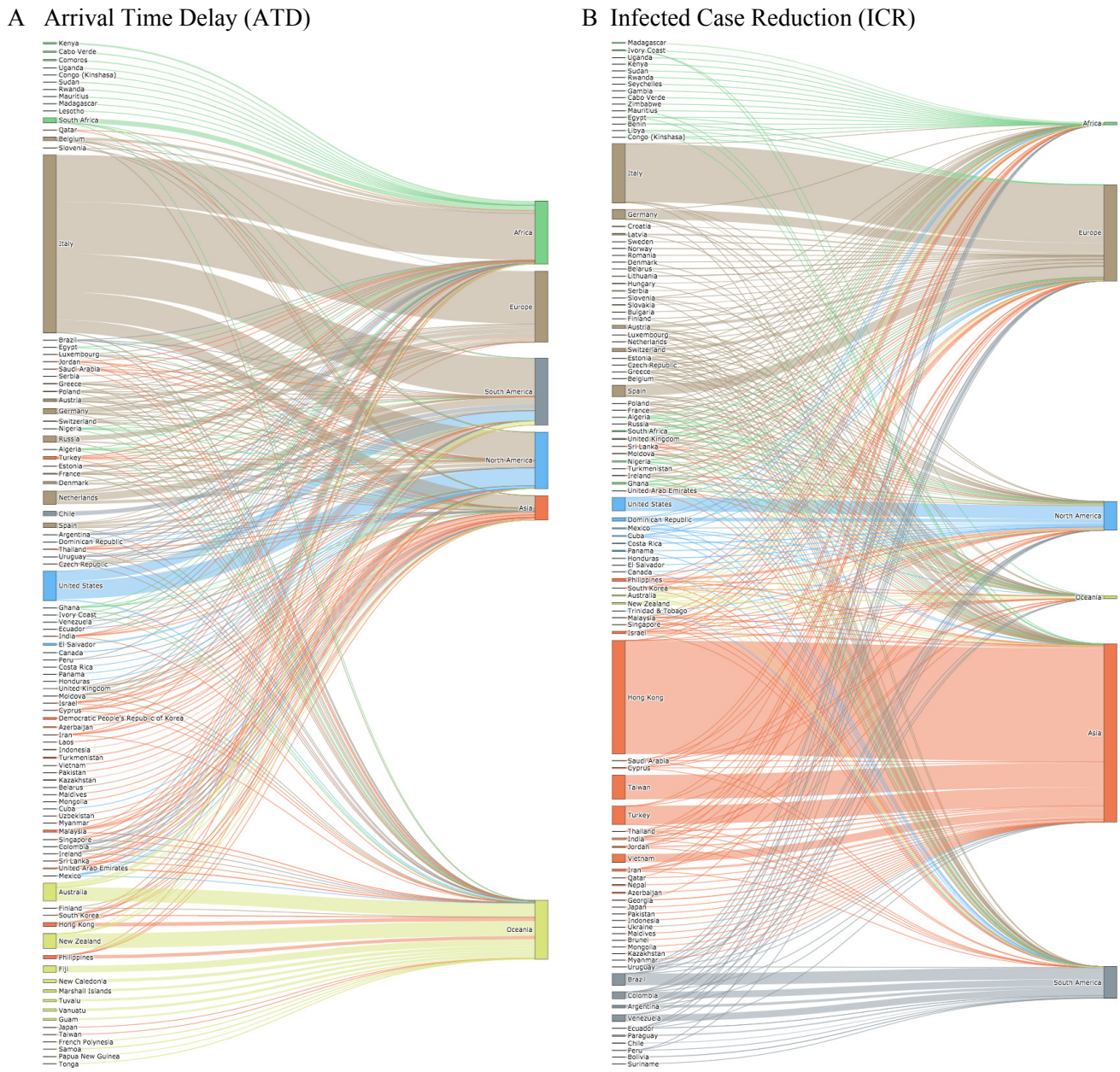

Figure S8: The arrival time delay (ATD) and infected case reduction (ICR) contribution of geographic areas (except for mainland China) to different continents till Apr-4. (A) ATD. (B) ICR. The flow from the left to the right implies the ATD and ICR to the right continents from the left areas' travel restrictions.

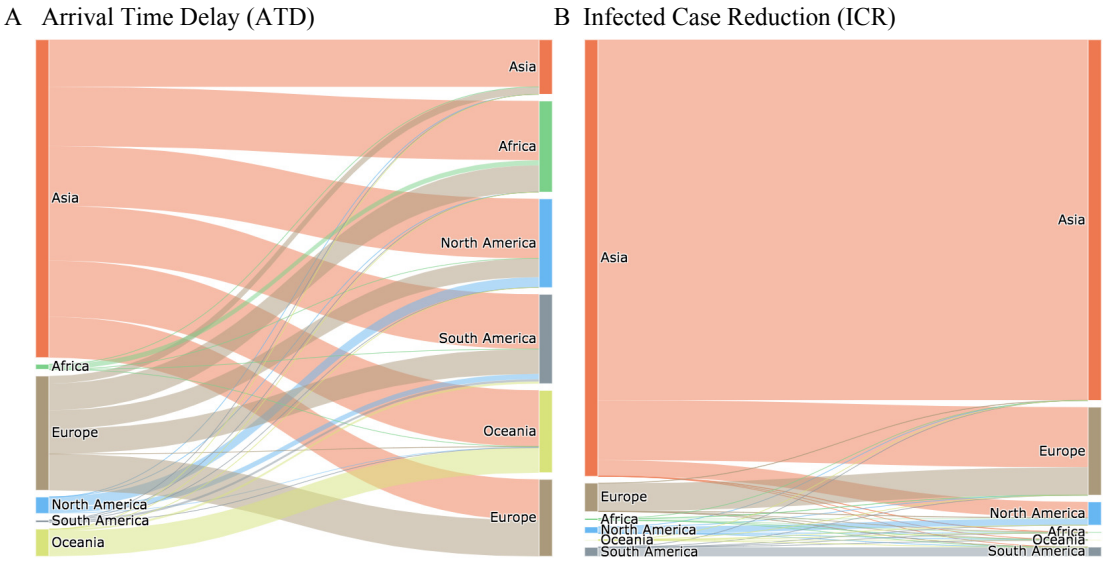

Figure S9: The arrival time delay (ATD) and infected case reduction (ICR) contribution between continents till Apr-4.

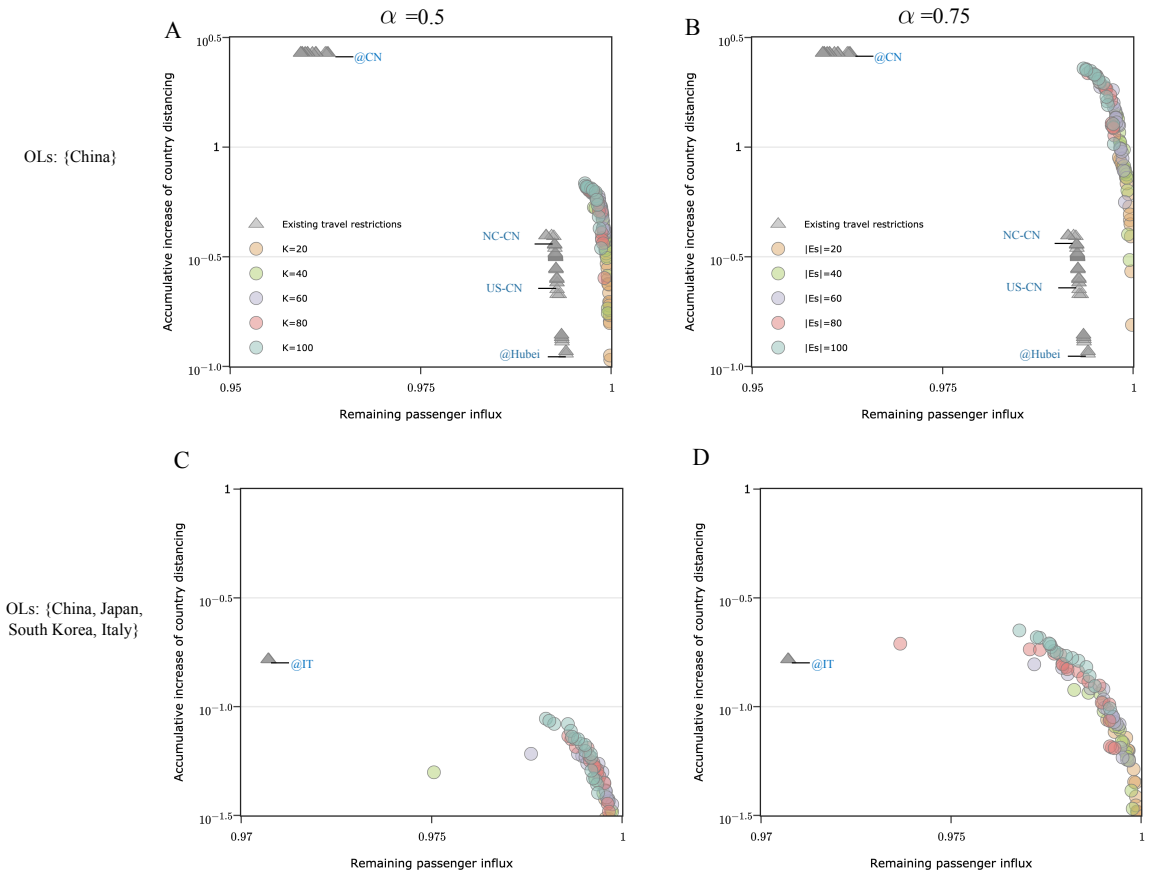

Figure S10: Non-dominated solutions with NSGA-II of the optimized travel restrictions which comprise different size ($K = 20, 40, 60, 100$) of entry bans when (A) OLs is {mainland China}, and α= 0.5; (B) OLs is {mainland China} and α= 0.9; (C) Multiple OLs is { mainland China, South Korea, Japan, Italy} and α= 0.5; (D) Multiple OLs is { mainland China, South Korea, Japan, Italy} and α= 0.9.

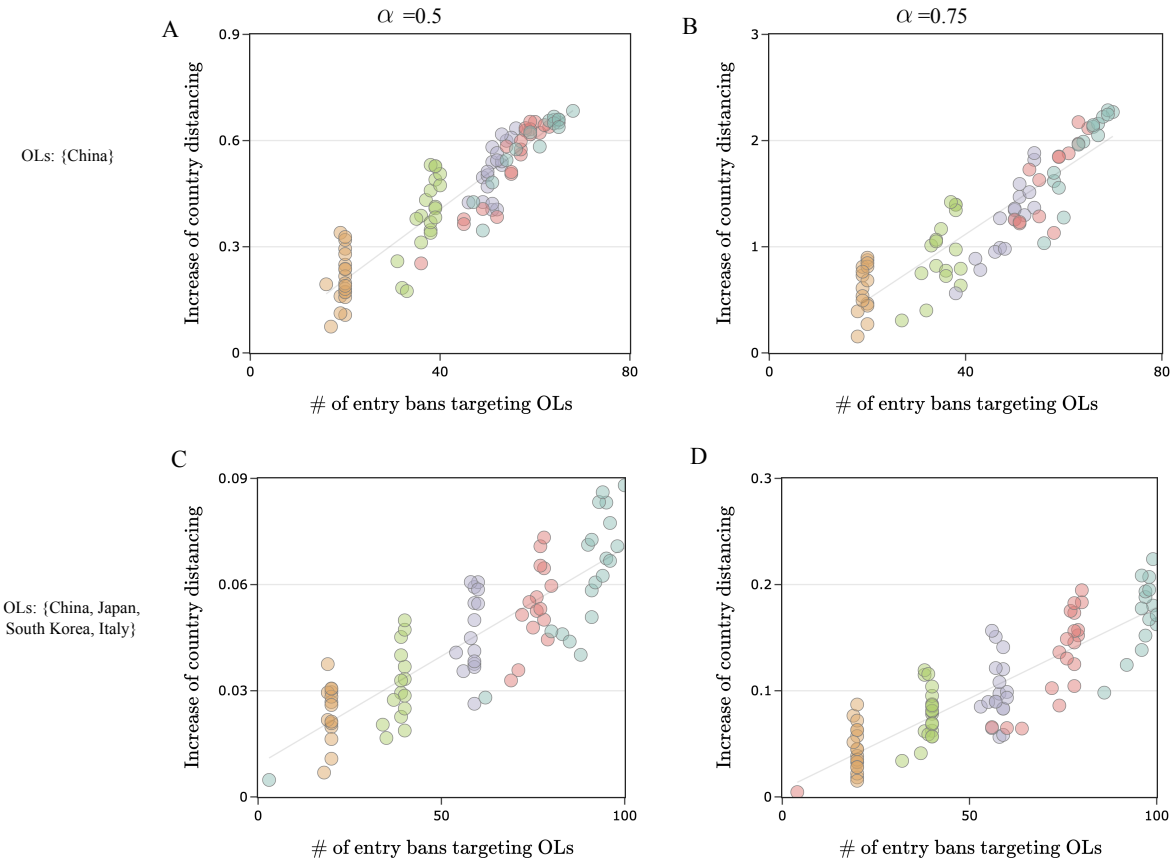

Figure S11: Correlation between the number of entry bans targeting OLs and the effectiveness of optimized travel restrictions which comprise different size ($K = 20, 40, 60, 80, 100$) of entry bans when (A) OLs is {mainland China}, and α= 0.5; (B) OLs is {mainland China} and α= 0.9; (C) Multiple OLs is { mainland China, South Korea, Japan, Italy} and α= 0.5; (D) Multiple OLs is { mainland China, South Korea, Japan, Italy} and α= 0.9.